Self-diffusion of Fe and Pt in $L1_0$-Ordered FePt: Molecular Dynamics simulation

S.I. Konorev [a], R. Kozubski [b],[*], M. Albrecht [c], I.A. Vladymyrskyi [a],[*]

[a] *Metal Physics Department, National Technical University of Ukraine "Igor Sikorsky Kyiv Polytechnic Institute", Prospect Peremogy 37, 03056 Kyiv, Ukraine*
[b] *M. Smoluchowski Institute of Physics, Jagiellonian University, Lojasiewicza 11, 30-348 Krakow, Poland*
[c] *Institute of Physics, University of Augsburg, Universitätsstraße 1, D-86159 Augsburg, Germany*

ABSTRACT

Vacancy-mediated lattice diffusion coefficients of Fe and Pt atoms in the chemically ordered $L1_0$-FePt phase at temperatures between 1300 and 1600 K were evaluated by means of Molecular Dynamics (MD) simulations. Due to the anisotropic structure of the $L1_0$-ordered FePt phase, Fe and Pt diffusion fluxes and the resulting self-diffusion coefficients were considered along and perpendicular to the [0 0 1] crystallographic direction. In view of a very low vacancy concentration in real FePt single crystals, steady state conditions of the simulated process were approximated by specifically scaling the self-diffusion coefficients estimated for higher vacancy concentrations to the equilibrium vacancy concentration. This procedure involved the calculation of vacancy formation energies which appeared temperature dependent. The validity of this approach was thoroughly tested and the final results were analyzed and compared to the relevant literature data. The evaluated temperature dependent Fe and Pt self-diffusion coefficients showed Arrhenius behavior, however, their values were much lower than the reported experimental ones. Apart from the inevitable effect of the applied quasi-empirical potentials, the discrepancies might originate from the fact that while the MD simulations addressed a single crystal of FePt defected exclusively with vacancies and antisites, the existence of fast diffusion paths along linear and planar defects cannot be excluded in real materials.

1. Introduction

Diffusion plays an important role in a large variety of processes in materials science [1]. In order to control diffusion and thus, to get a handle on various material properties, it is required that the underlying diffusion processes and their parameters are known.

The present paper reports on the results of atomistic simulation of self-diffusion in the intermetallic $L1_0$-FePt compound crystallizing in the face-centered tetragonal (fct) structure, where the tetragonal distortion results from the long-range $L1_0$-type chemical order with an alternating sequence of (0 0 1)-oriented Fe- and Pt-monatomic planes, as displayed in Fig. 1.

Despite the fact that $L1_0$-FePt thin films are used for ultrahigh density heat assisted magnetic recording [2–8], their physical properties regarding diffusion are to a large extent unexplored. The available data is mainly experimental. In this regard, Kucera and Million measured diffusion coefficients of Pt in polycrystalline Fe-Pt solid solutions in the concentration interval 15–60 at.% Pt (i.e. including $L1_0$-FePt) at

temperatures from 1050 K to 1690 K by means of a residual activity method, using the isotope ^{193}Pt [9]. The calculated temperature dependent diffusivities satisfied well the Arrhenius behavior, making it possible to estimate the pre-exponential factor and the activation energy. It was shown that $L1_0$-type chemical ordering at Pt concentration close to the equiatomic FePt stoichiometry leads to a sudden increase of the activation energy for diffusion. Kushida et al. measured diffusion coefficients of Fe in FePt in both ordered and disordered states [10]. A decrease of Fe diffusivity due to the ordering process was reported. Moreover, self-diffusion of Fe in the $L1_0$-FePt phase appeared anisotropic: a higher value of diffusion activation energy was found for diffusion along the [0 0 1] direction (3.8 eV) than for diffusion perpendicular to it (3.2 eV). Nosé et al. confirmed these results by means of tracer diffusion experiments performed at temperatures between 1222 K and 1663 K and showed that considerably faster diffusion of Fe atoms is observed perpendicular to the [0 0 1] direction [11]. A combination of nuclear resonant scattering (NRS) and nuclear tracer techniques allowed investigating diffusion characteristics at lower temperatures. For
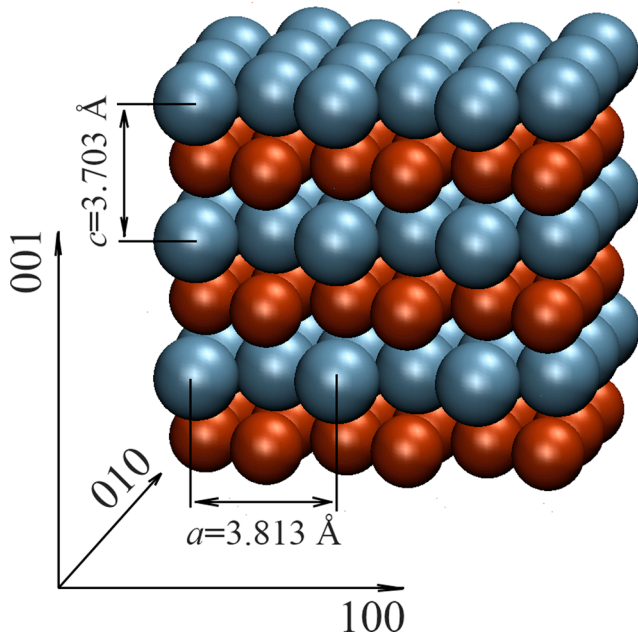
Fig. 1. Chemically ordered $L1_0$-structure of FePt. Blue and red spheres represent Fe and Pt atoms, respectively.

instance, tracer diffusion of Fe in $L1_0$-FePt thin films at temperatures from 773 K up to 873 K was investigated by Rennhofer et al. [12]. The activation energy of Fe diffusion calculated in their study in [001] direction (1.65 eV) resulted in more than two times lower values than previously measured in the high temperature regime (3.8 eV, [10]). The authors attributed this difference to different diffusion mechanisms dominating in both temperature intervals: highly correlated six-jumps cycles at lower temperatures and the antistructural bridge mechanism at higher temperatures. Moreover, Gröstlinger et al. [13], using also the NRS method, got some insight to the anisotropic diffusion of Fe in $L1_0$-FePt films at low temperatures (653 K−743 K). Again, the diffusion perpendicular to the [001] $L1_0$ direction ran by up to two orders of magnitude faster than along this direction.

Chemical depth profiling methods were also employed to study diffusion processes and solid state reactions in Fe/Pt based layer stacks upon annealing [14,15]. For instance, almost full diffusion homogenization of Pt/Fe bilayers at relatively low annealing temperatures (lower than 600 K) was observed by secondary neutral mass spectrometry in combination with x-ray diffraction, and transmission electron microscopy [16]. In this case, diffusion homogenization was interpreted as controlled by the grain-boundary-diffusion-induced reaction layer formation mechanism, where grain boundary diffusion leads to the movement of grain boundaries in the direction perpendicular to their initial plane, leaving behind an area of a homogeneous alloy [17]. Moreover, introduction of an additional Au intermediate layer between the Pt and Fe layers resulted in significant enhancement of low-temperature intermixing between Fe and Pt [18]. Application of *in-situ* resistivity measurements during heating of Pt/Fe bilayers in combination with chemical depth profiling and structural analysis provided additional valuable information concerning the development of diffusion processes, structural phase transitions, and its stability range [4].

Experimental investigation of diffusion process in nanoscale layer stacks is, however, difficult and in some cases even impossible, due to very small diffusion distances and very high process rates. Moreover, experimental techniques usually provide only information about effective diffusion parameters, i.e. values averaged over a large diffusion area and over a large number of atomic jumps contributing to the diffusion flux [19].

In this regard, computer simulations based on Monte Carlo (MC) and

Molecular Dynamics (MD) techniques are powerful tools for atomistic modelling of diffusion and diffusion-controlled phenomena in solids. The current development of MD methods allows analyzing various aspects of complex material processes such as structural modifications generated by stress, temperature, or structural defects [19].

The main advantage of MD simulations is the possibility to investigate material parameters in real time under dynamic conditions, e.g. at varying temperature or pressure. Besides, MD allows studying materials with diverse concentrations of structural defects. This advantage is extremely important for the investigation of diffusion processes since lattice diffusion in solids is mainly mediated by point defects and directly affected by the concentration of these defects. The above advantages of MD are, however, accompanied by mainly technical drawbacks such as very limited time scales feasible in the simulations and limited size of simulation cells. However, fast development of the computing power of contemporary machines considerably widened the power of MD algorithms and, in particular, made them useful for the modelling of atomic migration at larger time scales. For instance, Mendelev and Mishin evaluated self-diffusion of Fe in bcc Fe mediated by vacancies and interstitial atoms directly from MD simulations using semi-empirical interatomic potentials [20]. This approach appeared adequate to study both pure metals and alloys, e.g. Smirnova et al. applied classical MD to evaluate self-diffusion parameters in pure U and U-Mo alloys [21]. To the best of our knowledge, however, no systematic MD studies of diffusion in ordered intermetallics have been performed up to now.

The present study aims at filling this gap and shows the results of MD simulations of vacancy-mediated Fe- and Pt-self-diffusion in the chemically ordered $L1_0$-FePt intermetallic phase.

2. General approach

2.1. Atomistic approach: Einstein-Smoluchowski model

Self-diffusion of Fe- and Pt-atoms in the $L1_0$-FePt alloy is assumed to be controlled by vacancy-mediated random walk which justifies the evaluation of the related self-diffusion coefficients using the atomistic formalism developed by Einstein and Smoluchowski [22,23]. Since the crystal structure of the ordered $L1_0$-FePt phase consists of regularly alternating (001) monatomic Fe and Pt planes, leading to tetragonal distortion of the lattice along the [001] direction, diffusion has to be considered along and perpendicular to this direction. In the present work two independent diffusion coefficients were analyzed: $D^\parallel$ for diffusion in [001] direction and $D^\perp$ estimated as an average of the diffusivities along the [100] and [010] directions. The necessity for separate consideration of the two diffusivities also follows from different mechanisms of diffusion parallel to the monatomic planes ($D^\perp$, predominantly exchange between atoms of same elements) and perpendicular to those planes ($D^\parallel$, predominantly exchange between atoms of different elements). The corresponding diffusion coefficients of X-atoms (X = Fe; Pt) were evaluated from the standard Einstein-Smoluchowski relationship:

$$D_X^{\perp(\parallel)} = \frac{MSD_X^{\perp(\parallel)}(t)}{2t} \tag{1}$$

where $MSD_X^{\perp(\parallel)}(t)$ (X = Fe; Pt) denotes the mean square displacement of X-atoms achieved within the simulation time (t) in corresponding direction of the lattice, i.e. the corresponding squared displacement averaged over the total number of X-atoms in the sample. It should be noticed that $MSD_X^\perp(t)$ was evaluated as an average of MSD values obtained in [100] and [010] directions of the lattice.

2.2. Adequacy of MD

All MD simulations were performed by means of the Large-scale

Atomic/Molecular Massively Parallel Simulator (LAMMPS) software package [24,25]. The thermostatting and barostatting of the simulated NVT (constant number of atoms, volume and temperature) and NPT (constant number of atoms, pressure and temperature) ensembles was provided by LAMMPS [24] via correction of the atom velocities (thermostatting) and via correction of the volume of the simulation area (barostatting).

The adequacy of MD for the simulation of self-diffusion in the $L1_0$-FePt alloy was confirmed by showing that the technique reproduces atomic migration predominantly mediated by vacancies. The latter was demonstrated by performing a dedicated MD simulation where MSD of Fe atoms in [1 0 0] direction ($MSD_{Fe}^{(a)}$) was monitored at $T = 1600$ K in two $L1_0$-ordered FePt samples built of 12x12x12 fct cells, i.e. containing 6912 lattice sites. While one of the samples contained exclusively equal numbers of Fe and Pt atoms without defects, in the second sample 9 lattice sites selected at random were left empty (i.e. occupied by vacancies). 3D periodic boundary conditions were applied for both samples. Fig. 2 shows the corresponding $MSD_{Fe}^{(a)}(t)$ curves which clearly reveals that migration of Fe atoms is observed exclusively in the sample containing vacancies.

The $MSD(t)$ curves shown in Fig. 2, as well as in all other figures were generated by smoothening the raw MD data scattered due to thermal oscillations of the simulated atoms. The error bars are equal to the amplitudes of these oscillations.

While the continuous and smooth increase of $MSD_{Fe}^{(a)}(t)$ registered at the presence of vacancies indicates the occurrence of atomic jumps to vacancies, the very low values of this parameter show that during the simulation time only a small fraction of Fe atoms moved to neighboring lattice sites. Fig. 3 shows the time dependence of the fraction of Fe atoms in the sample displaced by more than one nearest neighbor (nn) distance in the $L1_0$-FePt structure. It is also important to note that due to correlation effects not all atom displacements lead to the increment of MSD: some of the moved atoms returned at the next step back to their initial positions without contributing to the increase in MSD.

It should be noted that the equilibrium atomic configuration of long-range ordered systems – covering temperature-dependent degree of long-range order of atoms and vacancies – builds up by vacancy-mediated atomic migration. Once the particular temperature is applied, the sample first tends to equilibrium which means that the observed atomic migration is not self-diffusion – defined as a steady-state process occurring in equilibrium atomic and defect configurations. This effect is reflected by the characteristic shape of the $MSD_X^{\perp(\parallel)}(t)$ curves which become linear starting only from a particular onset marking the establishment of the equilibrium configuration in the sys-
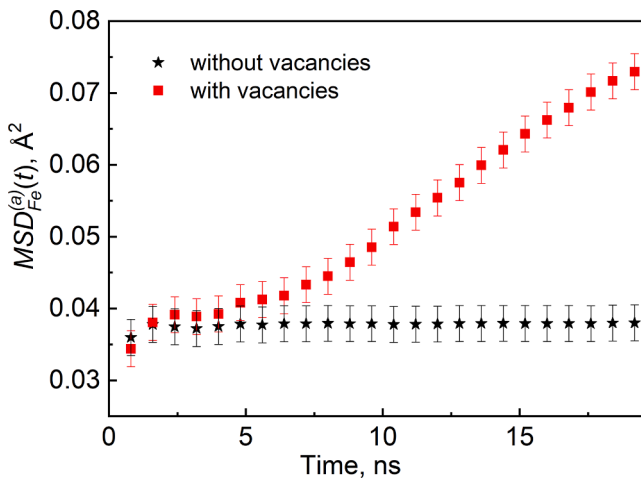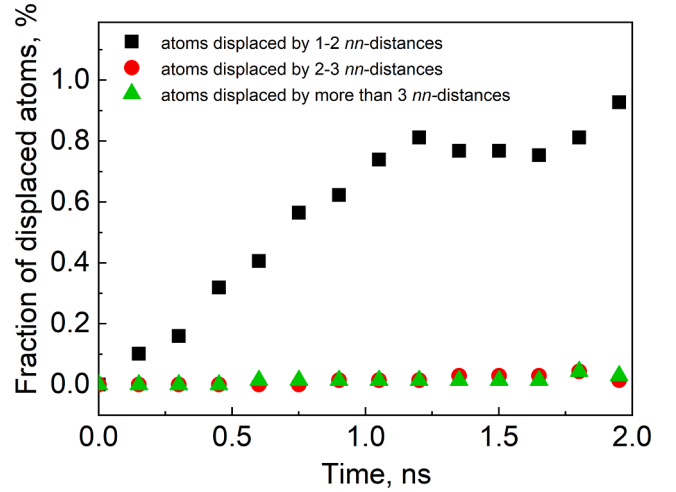

Fig. 3. Time-dependence of numbers of atoms displaced by more than one nearest neighbor (nn) distance at $T = 1600$ K.

tem. The $MSD_X^{\perp(\parallel)}(t)$ curves should, therefore, be analyzed carefully and self-diffusion constants should be evaluated by fitting only their linear segments at longer time scales (see Sections 4.2.1 and 4.2.2.).

2.3. General treatment of the effect of vacancies

The related atomistic theory [26] shows that slopes of $MSD_X(t)$ and consequently also the coefficients of vacancy-mediated self-diffusion D_X depend on the so-called vacancy-availability factor. In the case of low vacancy concentration, this dependence may be approximated by a proportionality to the vacancy concentration $C_V = \frac{N_V}{N}$, where N_V and N denote the number of vacancies and the total number of atoms in the system, respectively.

The latter was applied in order to work around the issue of very low equilibrium vacancy concentrations $C_V^{(eq)}$ in $L1_0$-FePt – substantially lower than 10^{-4} – the value of C_V corresponding to a single vacancy introduced to the simulated sample. The procedure was composed of two stages:

- Evaluation of the diffusivities $D_{X\_sim}^{\perp(\parallel)}$ by running MD simulations with the vacancy concentration C_{V_sim} high enough to generate interpretable $MSD_X^{\perp(\parallel)}(t)$ dependencies;
- Determination of the correct diffusion coefficients by normalizing $D_{X\_sim}^{\perp(\parallel)}$ to the equilibrium vacancy concentration $C_V^{(eq)}$:

$$D_X^{\perp(\parallel)} = D_{X\_sim}^{\perp(\parallel)} \frac{C_V^{(eq)}}{C_{V\_sim}} \qquad (2)$$

with $C_V^{(eq)}$ determined by means of a procedure described in Section 2.5.

Fig. 4 shows the values of $D_{Fe}^{\perp}$ and $D_{Fe}\parallel$ yielded by MD simulations of samples containing 1, 3, 9, 18, and 27 vacancies, (i.e. with $10^{-4} < C_{V\_sim} < 4 \times 10^{-3}$) at $T = 1600$ K.

Constant average values of $D_{Fe}^{\perp}$ and $D_{Fe}\parallel$, indicating their proportionality to C_V, was observed for samples containing not more than 9 vacancies. Therefore, all MD simulations were performed using sample boxes built of 12x12x12 $L1_0$-ordered fct unit cells and containing 9 vacancies.

In view of the total number of lattice sites ($N = 6912$) introduction of 9 vacancies perturbed the sample stoichiometry by not more than 0.13%.
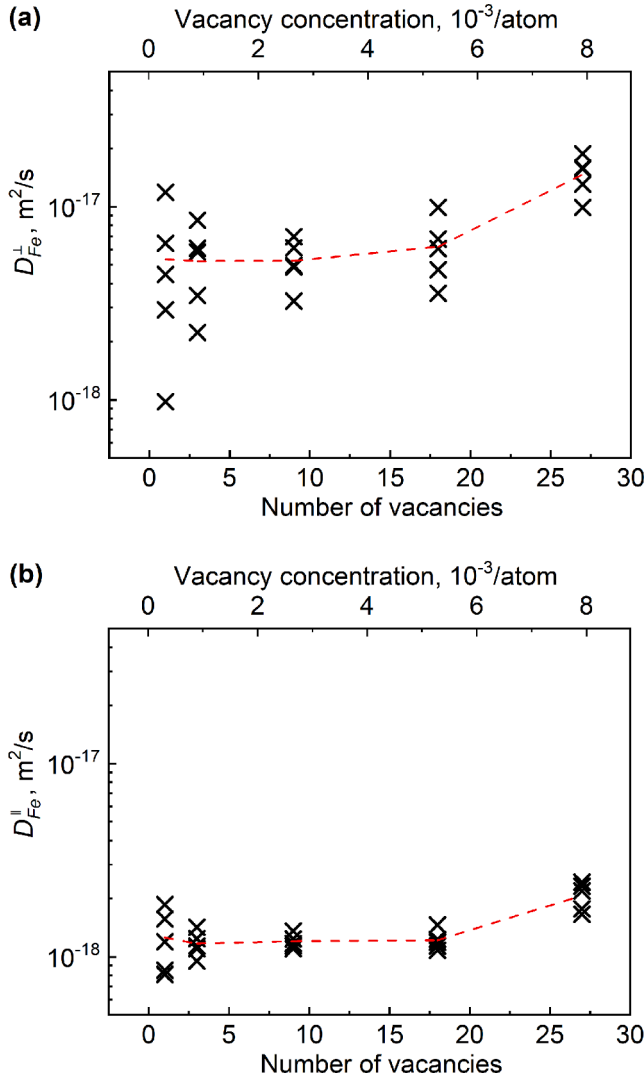

Fig. 2. Time dependence of $MSD_{Fe}^{(a)}$ in $L1_0$-ordered FePt with and without vacancies at $T = 1600$ K.

(a)

(b)

Fig. 4. Dependence of (a) $D_{Fe}^{\perp}$ and (b) $D_{Fe}^{\parallel}$ simulated at 1600 K on the number of vacancies introduced in the simulation sample box. Values obtained from single MD runs are marked by crosses while the dashed line traces the average values.

2.4. Effect of vacancies in $L1_0$-ordered binary systems on self-diffusion coefficient

In general, the chemical long-range order results in a specific distribution of vacancies in the sublattices. In the case of the $L1_0$-FePt binary alloy, it should be assumed that $C_{V_{Fe}}^{(eq)} \neq C_{V_{Pt}}^{(eq)}$, where $C_{V_X}^{(eq)} = \frac{N_{V_X}^{(eq)}}{N}$ (X = Fe, Pt) denotes the equilibrium concentration of vacancies residing on the X-sublattice and $N_{V_X}^{(eq)}$ is the equilibrium number of vacancies residing on the X-sublattice. It obviously holds $N_{V_X}^{(eq)} + N_{V_Y}^{(eq)} = N_V^{(eq)}$.

In view of the above feature, the method for the evaluation of $D_X^{\perp(\parallel)}$ based on Eq. (2) requires some clarification because the present procedure contains no definite criterion giving the initial distribution of vacancies in the Fe- and Pt-sublattices. A detailed analysis requires the determination of the equilibrium atomic/defect configuration feasible e. g. by means of Monte Carlo simulations (see [27]).

First, it was postulated that the following relationship holds:

$$MSD_X^{\perp(\parallel)} = MSD_{X\_V_X}^{\perp(\parallel)} + MSD_{X\_V_Y}^{\perp(\parallel)} \tag{3}$$

where $MSD_{X\_V_{X(Y)}}^{\perp(\parallel)}$ (X, Y = Fe, Pt) denotes the mean-square-displacement of X-atoms in particular crystallographic direction

observed in the case where all vacancies reside initially (i.e. at the beginning of the MD run) on X(Y)-sublattice sites.

According to the remarks of Section 2.3:

$$MSD_{X\_V_{X(Y)}}^{\perp(\parallel)} = N_{V_{X(Y)}} MSD_{X\_1V_{X(Y)}}^{\perp(\parallel)} \tag{4}$$

where $MSD_{X\_1V_{X(Y)}}^{\perp(\parallel)}$ denotes the mean-square-displacement of X-atoms, again in a particular direction, observed in the case where the sample box contains only one single vacancy initially residing on the X (Y)-sublattice site.

Combining Eqs. (3) and (4), one obtains

$$MSD_X^{\perp(\parallel)} = N_{V_X} MSD_{X\_1V_X}^{\perp(\parallel)} + N_{V_Y} MSD_{X\_1V_Y}^{\perp(\parallel)} \tag{5}$$

The validity of Eq. (5) was checked in a separate MD simulation of diffusion along the two considered directions of the $L1_0$-FePt structure (Fig. 5): $MSD_X^{\parallel}(t)$ and $MSD_X^{\perp}(t)$ were analyzed at 1600 K for three different cases: (i) the sample box contains 4 vacancies initially located on Fe sites of the $L1_0$ lattice; (ii) the sample box contains 4 vacancies initially located on Pt sites of the lattice, and (iii) the sample box contains 4 vacancies initially located on the Fe-sublattice and 4 vacancies initially located on the Pt sublattice. As can be seen in Fig. 5, MSD observed for the case (iii) can be reasonably approximated by the sum of MSDs obtained for the cases (i) and (ii).

The evaluation of correct and interpretable values of diffusion co-
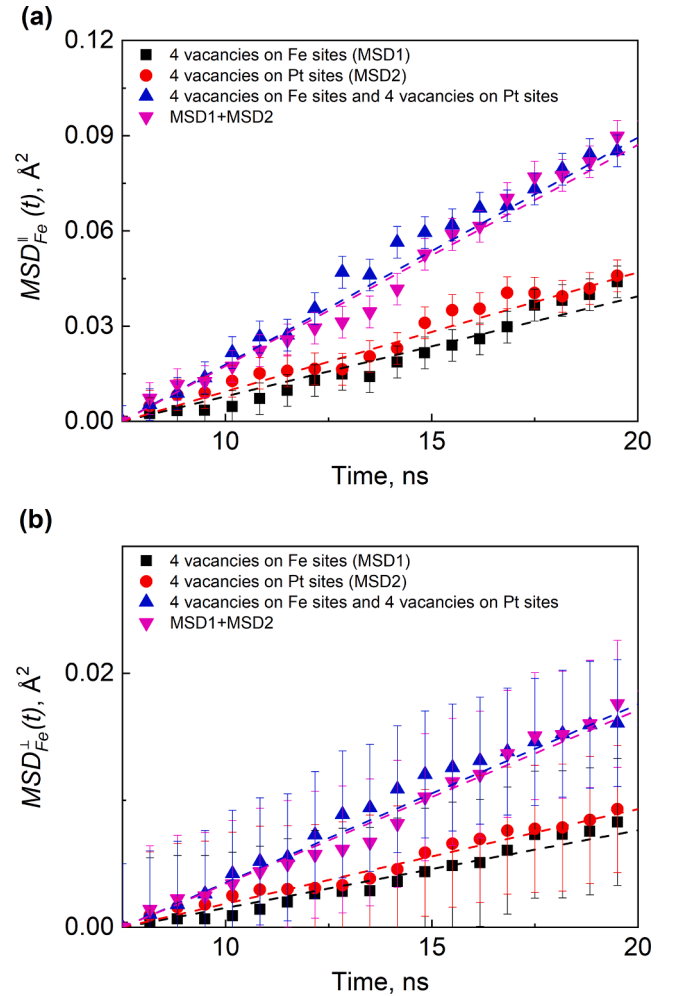
(a)

(b)

Fig. 5. Time dependence of the mean-square displacement of Fe atoms (a) perpendicular ($\perp$) and (b) parallel ($\parallel$) to the [0 0 1] direction of the $L1_0$-FePt structure at 1600 K for different numbers and different initial positions of vacancies in the sample box.

efficients requires that the simulations are performed with the numbers $N_{V_{Fe}}^{(eq)}$ and $N_{V_{Pt}}^{(eq)}$ of Fe- and Pt-vacancies corresponding to their equilibrium concentrations $C_{V_{Fe}}$ and $C_{V_{Pt}}$.

Considering Eqs. (1) and (5) as well as the definition of equilibrium vacancy concentration leads to the following formulas for diffusion coefficients in anisotropic crystals:

$$D_{Fe}^{\perp(\parallel)} = \frac{N_{V_{Fe}}^{(eq)} MSD_{Fe\_1V_{Fe}}^{\perp(\parallel)} + N_{V_{Pt}}^{(eq)} MSD_{Fe\_1V_{Pt}}^{\perp(\parallel)}}{2t}$$

$$= \frac{N}{2t}\left(C_{V_{Fe}}^{(eq)} MSD_{Fe\_1V_{Fe}}^{\perp(\parallel)} + C_{V_{Pt}}^{(eq)} MSD_{Fe\_1V_{Pt}}^{\perp(\parallel)} \right), \tag{6}$$

$$D_{Pt}^{\perp(\parallel)} = \frac{N_{V_{Fe}}^{(eq)} MSD_{Pt\_1V_{Fe}}^{\perp(\parallel)} + N_{V_{Pt}}^{(eq)} MSD_{Pt\_1V_{Pt}}^{\perp(\parallel)}}{2t}$$

$$= \frac{N}{2t}\left(C_{V_{Fe}}^{(eq)} MSD_{Pt\_1V_{Fe}}^{\perp(\parallel)} + C_{V_{Pt}}^{(eq)} MSD_{Pt\_1V_{Pt}}^{\perp(\parallel)} \right) \tag{7}$$

Thus, the task of diffusion coefficient calculation comes down to two tasks: (i) evaluation of equilibrium vacancy concentrations $C_{V_{Fe}}^{(eq)}$ and $C_{V_{Pt}}^{(eq)}$, and (ii) evaluation of the mean-square-distances $MSD_{Fe\_1V_{Fe}}^{\perp(\parallel)}$, $MSD_{Fe\_1V_{Pt}}^{\perp(\parallel)}$, $MSD_{Pt\_1V_{Fe}}^{\perp(\parallel)}$, and $MSD_{Pt\_1V_{Pt}}^{\perp(\parallel)}$, as defined above.

2.5. Evaluation of equilibrium vacancy concentration

The equilibrium vacancy concentration ($C_V^{(eq)}$) and its temperature dependence are associated with the change of Gibbs free energy (G_V) due to the formation of a single vacancy [28] given by:

$$C_V^{(eq)} = exp(-G_V/k_BT) = exp(-(E_V - TS_V)/k_BT), \tag{8}$$

where E_V, S_V, k_B, and T denote the vacancy formation energy, vacancy formation entropy, Boltzmann constant, and absolute temperature, respectively.

The vacancy formation energy E_V was evaluated using Eq. (9) valid for single-component systems [29]:

$$E_V = E_d - E_i \frac{N-1}{N}, \tag{9}$$

where E_d and E_i denote total energies of the system with and without a single vacancy, respectively, while N is the number of atoms in the sample.

Multicomponent systems require distinction between the types of vacancies (i.e. types of atoms which they replace). It is, therefore, convenient to rewrite Eq. (9) in terms of the average potential energy E_a of the particular atom replaced by a vacancy:

$$E_V = E_d - (E_i - E_a) \tag{10}$$

This approach was thoroughly tested and successfully applied to investigate diffusion in pure metals [20] and alloys [21].

In the case of perfectly $L1_0$-ordered FePt alloys, Eq. (10) yields the formation energies for Fe ($E_V^{(Fe)}$) and Pt ($E_V^{(Pt)}$) vacancies.

In the present work, the formation energies $E_v^{(Fe)}$ and $E_v^{(Pt)}$ were evaluated by running NVT-ensemble MD simulations covering the time of 5 ns and using time steps of 10^{-15} s at temperatures ranging from 300 K to 1600 K. Three systems were simulated: (i) one without vacancies; (ii) one with a single Fe-vacancy, and (iii) one with a single Pt-vacancy. The results were averaged over 8 independent simulation runs with different initial velocities of the atoms. When simulating the systems (ii) and (iii), the size of the sample box was chosen to be large enough, so that the effect of the vacancy introduced to the center of the box does not reach borders of this box. The later was controlled by the analysis of stresses which are almost equal to zero in the defect-free crystal. Introduction of a vacancy leads to the appearance of stresses, whose values again tend to zero at distances higher than two lattice spacings from the defect. In this case the application of NVT and NPT ensembles is equally possible due to the constant volume of the system. The NVT ensemble was used since it provides lower energy oscillations allowing to estimate the vacancy formation energy with higher accuracy. Please note that the exact calculation of the vacancy formation entropy S_V in FePt was beyond the scope of the present study.

The applied strategy consisted of first calculating $C_V^{(eq)}(T)$ with $S_V = 0$

$$C_V^{(eq)}(T) \approx exp\left(-E_V^{(X)}/k_BT\right); X = Fe; Pt \tag{11}$$

which provides the approximated temperature dependence of the equilibrium vacancy concentration. The possible effect of S_V on the present results was estimated by using the average value $S_V \approx 2k_B$ reported for fcc metals [30] which, according to Eq. (8), yielded a fixed coefficient e^2 in Eq. (11). The effect of this coefficient on the evaluated parameters will be discussed in Sections 3.1 and 4.2.

Table 1
Structural parameters of pure α-Fe and fcc Pt, as well as of $L1_2$-FePt$_3$, $L1_2$-Fe$_3$Pt, and $L1_0$-FePt evaluated in the present study using MEAM potentials [31] and corresponding literature data.

Parameter	Present study	Literature data	
α-Fe			
a, Å	2.873	2.8681 (experimental [35])	2.8664 (experimental [36])
cohesive energy, eV/atom	4.21	4.46 (ab-initio simulation [37])	4.28 (experimental [38])
thermal expansion coefficient, K^{-1}	12.1×10^{-6}	14×10^{-6} (experimental [32])	11.8×10^{-6} (experimental [39])
Pt			
a, Å	3.929	3.924 (experimental [40])	3.9241 (experimental [41])
cohesive energy, eV/atom	5.69	5.859 (experimental [37])	5.29 (simulation [42])
thermal expansion coefficient, K^{-1}	8.8×10^{-6}	8.93×10^{-6} (calculation [43])	8.921×10^{-6} (experimental [44])
$L1_2$-FePt$_3$			
a, Å	3.854	3.86 (experimental [45])	3.85 (experimental [46])
$L1_2$-Fe$_3$Pt			
a, Å	3.707	3.73 (experimental [46])	3.738 (experimental [47])
$L1_0$-FePt			
a, Å	3.813	3.869 (ab-initio simulation [48])	3.86 (experimental [49])
c, Å	3.703	3.769 (ab-initio simulation [48])	3.71 (experimental [49])
c/a	0.971	0.974 (ab-initio simulation [48])	0.961 (experimental [49])
T_m, K	1960	1838 [34]	
$T_{order-disorder}$, K	–	1573 ± 25 (MEAM calculation [31])	1573 (experimental [34])

3. Preliminary simulations

3.1. Reliability test

The Fe-Pt system was modelled employing 'modified embedded-atom method' (MEAM) potentials elaborated by Kim et al. [31] who extensively tested the potentials reproducing the experimental thermodynamic properties of Fe-Pt, including lattice parameters, bulk modulus, and the 'order-disorder' transition temperature.

The reliability of the applied potentials was tested also in the present study by calculating the temperature dependent lattice parameters, thermal expansion coefficients, and cohesive energies of body centered cubic (bcc) α-Fe and face centered cubic (fcc) Pt, as well as of $L1_2$-FePt$_3$, $L1_2$-Fe$_3$Pt, and $L1_0$-FePt. Reasonable agreement with the literature data was achieved (see Table 1). For instance, in the case of α-Fe, the calculated lattice constant deviated by less than 0.5% from the values deduced from experiments based on thermal expansion [32]. In addition to the literature data, the melting point T_m of FePt was evaluated by simulating the coexistence between the solid and liquid phases [33]. The simulated value of $T_m = 1960$ K appeared, however, by about 7% higher than the experimental one (1838 K [34]).

3.2. Determination of the simulation time step

It is essential that the MD simulation time step is substantially shorter than the period of atomic thermal vibrations. Too long time steps generate an increase of the system energy and thus, the suitability of the steps is tested by energy monitoring [50]. As the frequency of atomic vibrations depends on the atomic mass, the MD simulation time step must be thoroughly adjusted to the particular system.

In order to provide high accuracy of the evaluated parameters, all MD simulations were carried out with the same time step of $dt = 10^{-15}$ s, determined for Fe-atoms at 1600 K.

3.3. Calculation of equilibrium lattice parameters

Precise evaluation of the equilibrium lattice parameters of the investigated system is crucial for the reliability of the simulation of diffusion processes. Temperature dependence of the equilibrium lattice parameters of $L1_0$-FePt (providing zero values of stresses averaged in time) was determined by relaxing an ideal system without vacancies. This means that no fast diffusion paths were available which, together with the limited simulation time (~0.5 ns), eliminated any atom displacements between crystal planes and, therefore, the generation of

antisite defects. Fig. 6 shows the obtained curves which reveal a considerable anisotropy of thermal expansion of the system reflected by a gradual decay of the tetragonal distortion (i.e., the difference between the lattice parameters a and c) with increasing temperature. Reliability of the result obtained by simulating the ideal crystal is supported by the very low vacancy concentration observed in real crystals of $L1_0$-FePt: $C_V^{(eq)} \approx 10^{-8}$ at $T = 1600$ K (see next section).

The results shown in Fig. 6 substantially differ from those following from experimental investigations [51,52] showing a much stronger expansion in $a(b)$-direction than in c-direction. The cited works, however, investigated doped thin foils, in addition, with diverse admixtures.

4. Results of the main simulations

4.1. Equilibrium vacancy thermodynamics

Temperature dependences of the evaluated vacancy formation energies $E_V^{(Fe)}$ and $E_V^{(Pt)}$ are displayed in Fig. 7.

Both curves show that the increasing temperature generates not only a gradual increase of $E_V^{(Fe(Pt))}$, but also a reduction of $\left| E_V^{(Fe)} - E_V^{(Pt)} \right|$. It should be noted that a continuous increase of the vacancy formation energy with increasing temperature has been reported in the literature also for other systems (see e.g. Ref. [20,53,54]). Extrapolation of $E_V^{(Fe)}(T)$ and $E_V^{(Pt)}(T)$ to $T \to 0$ K yields values of 2.53 eV and 2.31 eV for $E_V^{(Fe)}$ and $E_V^{(Pt)}$, respectively.

Fig. 8 shows the temperature dependences of $C_{V_{Fe}}^{(eq)}$ and $C_{V_{Pt}}^{(eq)}$ evaluated using eq. (11) including the related temperature-dependent vacancy formation energies $E_V^{(Fe)}$ and $E_V^{(Pt)}$ (Fig. 7).

The values of $\langle E_V^{(Fe)} \rangle$ and $\langle E_V^{(Pt)} \rangle$ estimated from the slopes of the corresponding Arrhenius plots (Fig. 8b), i.e. specific averages over the temperature-dependent vacancy-formation energies displayed in Fig. 7, were equal to 2.582 eV and 2.378 eV, respectively. Higher values of $E_V^{(Fe)}$ with respect to $E_V^{(Pt)}$ resulted in $C_{V_{Fe}}^{(eq)} < C_{V_{Pt}}^{(eq)}$, which is valid for all temperatures investigated.

As announced in Section 2.5, the $C_{V_X}^{(eq)}(T)$ curves traced in Fig. 8 were determined by neglecting the vacancy formation entropy S_V. The range of the corresponding error, i.e. the underestimation of $C_{V_X}^{(eq)}(T)$, is visualized in Fig. 9 where the curves of Fig. 8 are plotted together with the ones showing $C_{V_X}^{(eq)}(T)$ multiplied by a factor e^2.

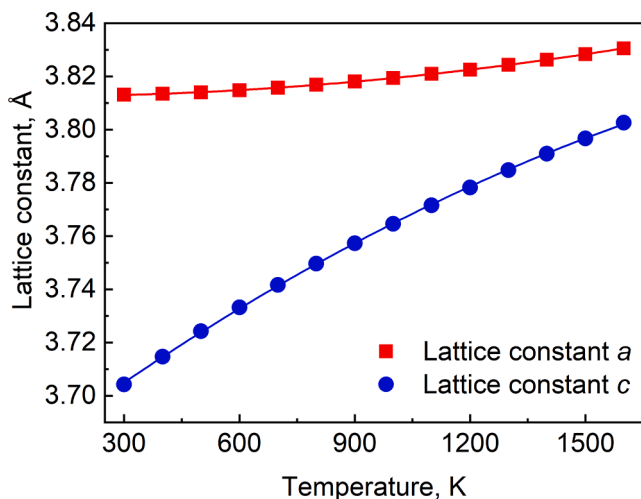Although no qualitative effect of the correction on the shape of the

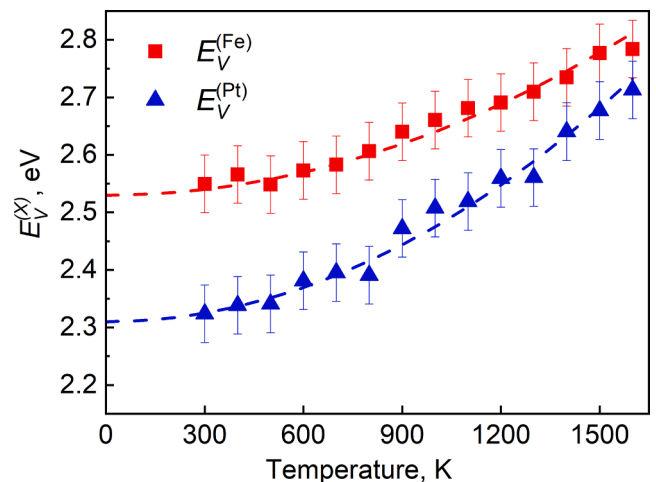**Fig. 6.** Temperature dependence of the lattice constants of $L1_0$-FePt determined by MD simulations.

Fig. 7. Temperature dependence of Fe- and Pt-vacancy formation energies in $L1_0$-ordered FePt.
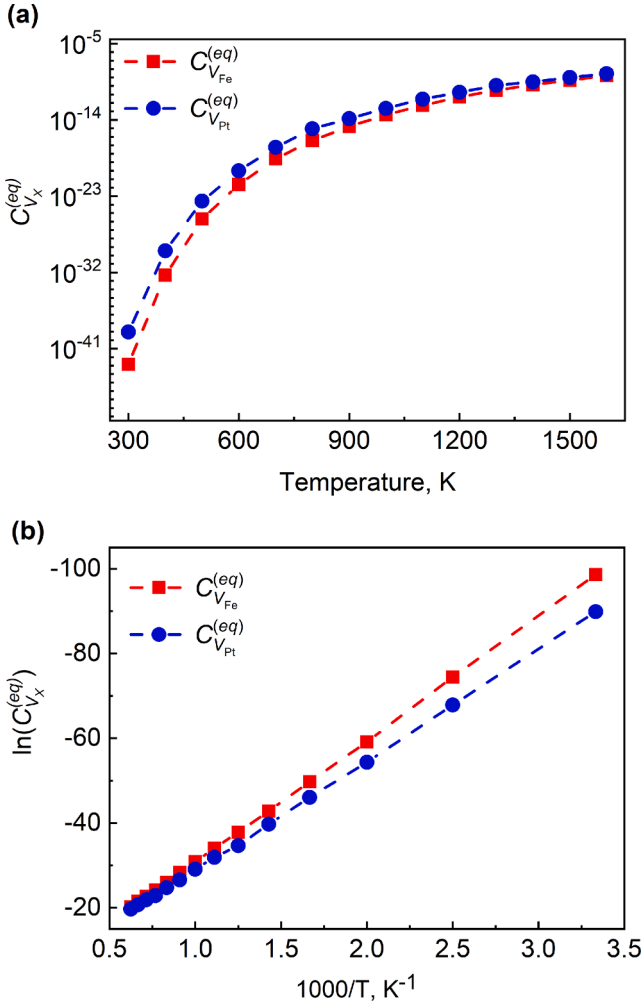
(a)

(b)

Fig. 8. (a) Temperature dependence of the equilibrium vacancy concentrations on Fe- and Pt-sublattices in $L1_0$-FePt and (b) corresponding Arrhenius plot.
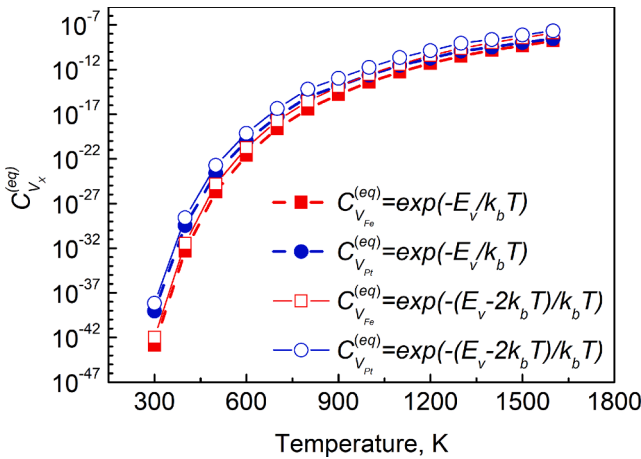

Fig. 9. Comparison of temperature dependences of the equilibrium vacancy concentrations on Fe- and Pt-sublattices in $L1_0$-FePt calculated by Eqs. (11) and (8), assuming that entropy of vacancy formation is equal to 2 k_b.

curves is visible, it is clear that the underestimation of $C_{V_X}^{(eq)}$ calculated with $S_V = 0$ will automatically generate an underestimation of the diffusion coefficients $D_X^{\perp(\parallel)}$ determined by Eq. (2).

4.2. Self-diffusion coefficients of Fe- and Pt-atoms

4.2.1. Evaluation of mean-square distances travelled by Fe- and Pt-atoms

Time-dependences of the mean-square distances $MSD_{X\_9V_Y}^{\perp(\parallel)}(t)$ travelled by X-atoms in samples containing 9 vacancies initially residing on Y-sublattice sites (X, Y = Fe, Pt) were determined for temperatures ranging from 1400 K to 1600 K by running 2,000,000 MD steps (20 ns in real time) performed with the same parameters as those applied when evaluating the vacancy formation energy. Each $MSD_{X\_9V_Y}^{\perp(\parallel)}(t)$ curve was corrected for thermal vibrations of atoms around the lattice sites as well as for a collective drift of atoms occurring in MD simulations of systems with periodic boundary conditions. The latter was done by correcting $MSD_{X\_9V_Y}^{\perp(\parallel)}(t)$ for the movement of the mass center of the sample.

In order to subtract the contribution of thermal vibrations, two types of curves, $MSD_{X\_9V_Y}^{\perp(\parallel)}(t)$ and $MSD_{X\_9V_Y}^{\perp(\parallel)(vib)}(t)$, were registered by simulating systems with and without vacancies, respectively. In case of the system containing no vacancies, no diffusion of atoms occurs and hence, the curves $MSD_{X\_9V_Y}^{\perp(\parallel)(vib)}(t)$ (see the curve displayed in Fig. 2) were mostly flat with only an initial increase caused by the relaxation of the system (i.e. equilibration of atom positions and velocities) (see [55;56]). Thus, 'corrected' curves $MSD_X^{\perp(\parallel)(corr)}(t) = MSD_X^{\perp(\parallel)}(t) - MSD_X^{\perp(\parallel)(vib)}(t)$ were used for further analysis.

Fig. 10a and 10b show the $MSD_{Fe\_9V_{Fe}}^{\perp(\parallel)}(t)$ dependences obtained at four different temperatures. The same curves corrected for thermal vibrations – $MSD_{Fe\_9V_{Fe}}^{\perp(\parallel)(corr)}(t)$ – are displayed in Fig. 10c and 10d. As explained above, no vacancy-mediated atomic migration was observed at 1300 K and the initial increase of $MSD_{Fe\_9V_{Fe}}^{\perp(\parallel)}(t)$ reflects equilibration of atom positions and velocities in the system. An increase of temperature leads to an increase of the slope of $MSD_{Fe\_9V_{Fe}}^{\perp(\parallel)}(t)$, which signalizes real atomic migration. The initial increase of $MSD_{Fe\_9V_{Fe}}^{\perp(\parallel)}(t)$ observed at 1300 K and attributed to the equilibration of atom positions and velocities is still visible in the "raw" curves corresponding to higher temperatures, but disappears after the correction for thermal vibrations. This indicates that the process of equilibration of atom positions and velocities is almost insensitive to temperature.

The different slopes of the $MSD_{Fe\_9V_{Fe}}^{\perp}(t)$ curves mark three distinct regimes of atomic migration – visible at all investigated temperatures.

The effect is especially well pronounced at 1600 K. Regimes I (~0–2 ns) and II (~2–7.5 ns) are associated with the relaxation of the system. As explained above, during the first relaxation stage (regime I) atoms and vacancies move to their optimal positions of the lattice corresponding to minimum energy of the system. In this case, distances travelled by atoms are much smaller than the lattice constant and the motion is not vacancy-mediated. According to previous studies (see [57]), the relaxation corresponding to the second stage (regime II) corresponds to vacancy-mediated redistribution of atoms towards the equilibrium degree of long-range order. Finally, regime III (greater than 7.5 ns) reflects a pronounced stationary self-diffusion process running in the system with equilibrium atomic configuration corresponding to the current temperature.

The observation that the time needed for equilibration of the system (onset of the linearity of $MSD_{Fe\_9V_{Fe}}^{\perp}(t)$) decreases with increasing temperature (~7.5 ns at 1600 K, ~13 ns at 1500 K, ~17 ns at 1400 K) supports the above interpretation which applies also to all the simulated $MSD_{X(Y)\_9V_{X(Y)}}^{\perp(\parallel)}(t)$ curves. Consequently, the Fe and Pt diffusivities $D_{Fe(Pt)}^{\perp(\parallel)}$ were deduced from the analysis of the latest linear part (regime III) of the relevant $MSD_{X(Y)\_9V_{X(Y)}}^{\perp(\parallel)}(t)$ curves.

4.2.2. Evaluation of self-diffusion coefficients

The values of diffusion coefficients $D_{Fe}^{\perp}$, $D_{Fe}\parallel$, $D_{Pt}^{\perp}$, and $D_{Pt}\parallel$ in $L1_0$-FePt estimated by means of the MD simulations at temperatures of 1400
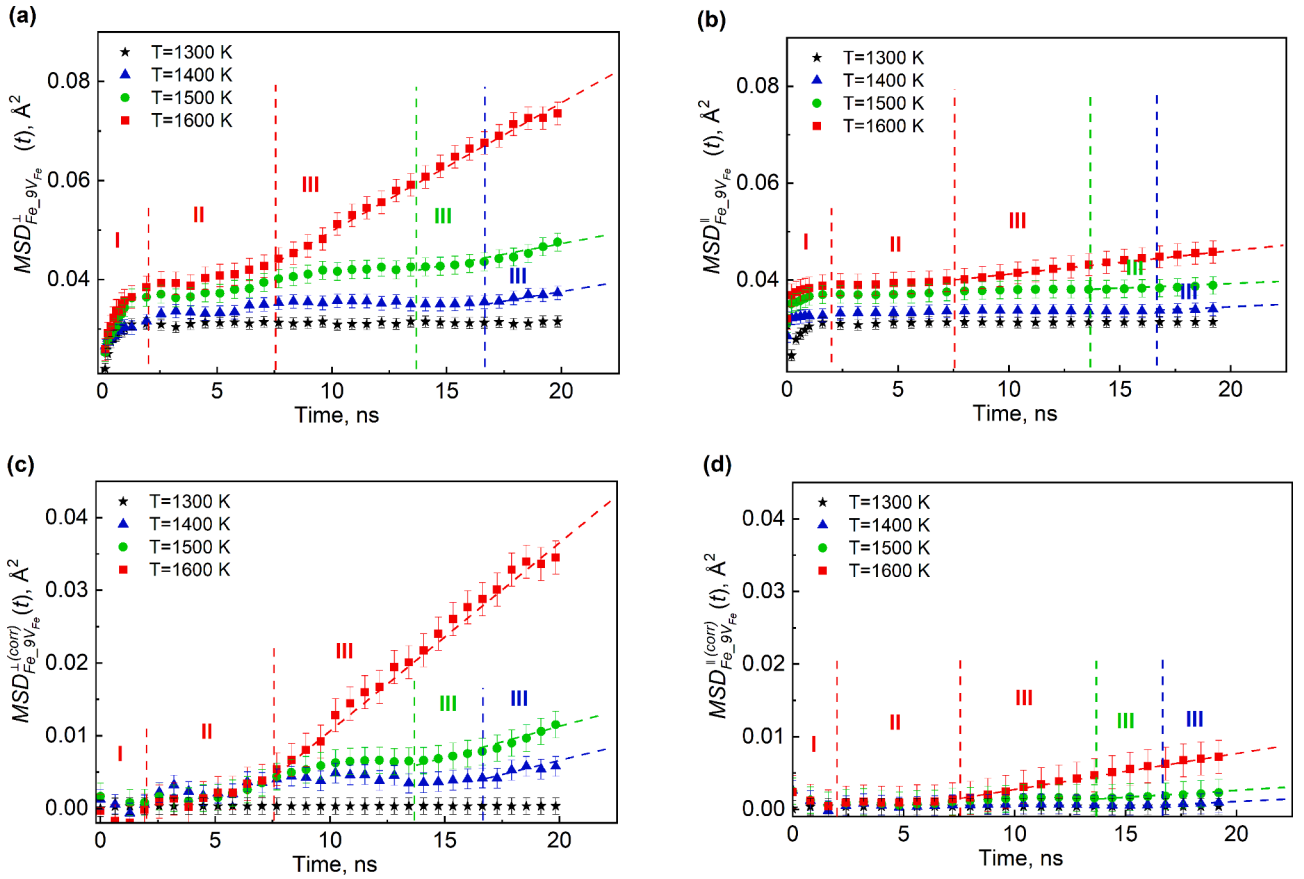
Fig. 10. Time dependence of (a) $MSD^\perp_{Fe\_9V_{Fe}}(t)$ and (b) $MSD_{Fe\_9V_{Fe}}\|(t)$ at four different temperatures. The same curves corrected for thermal vibrations are displayed in the graphs (c) and (d). Three different regimes (I-III) are marked.

Table 2
Self-diffusion coefficients of Fe and Pt atoms in $L1_0$-FePt estimated by means of the MD simulations at temperatures 1400 K, 1500 K, and 1600 K.

T, K	$D^\perp_{Fe}$, m²/s	$D_{Fe}\|$, m²/s	$D^\perp_{Pt}$, m²/s	$D_{Pt}\|$, m²/s
1400	$(7.5 \pm 2.6) \times 10^{-20}$	$(1.5 \pm 2.6) \times 10^{-20}$	$(2.6 \pm 2.6) \times 10^{-20}$	$(0.5 \pm 2.6) \times 10^{-20}$
1500	$(6.7 \pm 1.8) \times 10^{-19}$	$(1.3 \pm 1.8) \times 10^{-19}$	$(3.0 \pm 1.8) \times 10^{-19}$	$(0.6 \pm 1.8) \times 10^{-19}$
1600	$(5.2 \pm 1.2) \times 10^{-18}$	$(1.0 \pm 1.2) \times 10^{-18}$	$(3.3 \pm 1.2) \times 10^{-18}$	$(0.65 \pm 1.2) \times 10^{-18}$

K, 1500 K, and 1600 K are displayed in Table 2.

The corresponding Arrhenius plots are presented in Fig. 11 and yield the following values $Q_X^{\perp(\|)}$ of the activation energies for Fe and Pt diffusion in both considered crystallographic directions: $Q^\perp_{Fe} = 4.09 \pm 0.3$eV, $Q_{Fe}\| = 4.06 \pm 0.3$ eV and $Q^\perp_{Pt} = 4.67 \pm 0.4$ eV, $Q_{Pt}\| = 4.69 \pm 0.4$ eV.

As follows from Table 2, although the values of all the simulated self-diffusion coefficients corresponding to particular temperatures are in a similar range, D_{Fe} is always higher than D_{Pt}. For both Fe and Pt, self-diffusion runs about five times faster perpendicular to the [001] direction than along this direction.

5. Discussion

5.1. General remarks

The coefficients $D_{Fe}^{\perp(\|)}$ and $D_{Pt}^{\perp(\|)}$ of vacancy-mediated self-diffusion for Fe- and Pt-atoms in $L1_0$-FePt moving in [001] direction and perpendicular to it at temperatures between 1300 K and 1600 K were evaluated from the Einstein-Smoluchowski relationship (Eq. (1)). The
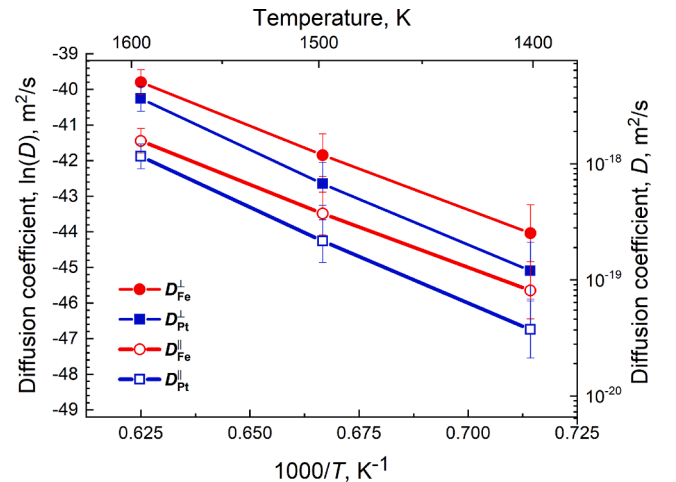

Fig. 11. Arrhenius plot of the self-diffusion coefficients $D^\perp_{Fe}$, $D_{Fe}\|$, $D^\perp_{Pt}$, and $D_{Pt}\|$ of $L1_0$-FePt.

Table 3

Overview of the self-diffusion coefficients $D_{Fe(Pt)}^{\perp(\|)}$, activation energies $Q_{Fe(Pt)}^{\perp\|}$ and pre-exponential factors D_0 of $L1_0$-FePt evaluated within the present MD simulations and experimental data reported in the literature.

D_{Fe}

$D^\perp$, present MD study

T, K	D, m²/s	Q, eV	D_0, m²/s
1400	$(7.5 \pm 2.6) \times 10^{-20}$	4.09 ± 0.3	$(3.82 \pm 0.2) \times 10^{-5}$
1500	$(6.7 \pm 1.8) \times 10^{-19}$		
1600	$(5.2 \pm 1.2) \times 10^{-18}$		

$D\|$, present MD study

T, K	D, m²/s	Q, eV	D_0, m²/s
1400	$(1.5 \pm 2.6) \times 10^{-20}$	4.06 ± 0.3	$(5.55 \pm 2.0) \times 10^{-6}$
1500	$(1.3 \pm 1.8) \times 10^{-19}$		
1600	$(1.0 \pm 1.2) \times 10^{-18}$		

Experimental data

T, K	D, m²/s	Q, eV	D_0, m²/s
$D\|$ [12]			
773	7.27×10^{-24}	1.65 ± 0.29	$(3.45 \pm 0.44) \times 10^{-13}$
823	2.09×10^{-23}		
848	7.73×10^{-23}		
873	1.05×10^{-22}		
$D^\perp$ Fe₅₄Pt₄₆ [11]			
1173	2.24×10^{-18}	3.38 ± 0.23	2.53×10^{-3}
1273	1.98×10^{-17}		
1323	6.48×10^{-17}		
1373	2.72×10^{-16}		
$D\|$ Fe₅₄Pt₄₆ [11]			
1173	1.20×10^{-18}	3.59 ± 0.21	4.35×10^{-2}
1273	1.20×10^{-17}		
1323	6.48×10^{-17}		
1373	2.25×10^{-16}		
$D^\perp$ [10]			
1333	5.88×10^{-16}	3.17 ± 0.36	6.76×10^{-4}
1393	2.5×10^{-15}		
1423	4.95×10^{-15}		
1493	1.1×10^{-14}		
$D\|$ [10]			
1333	2.5×10^{-16}	3.8 ± 0.45	0.07
1393	1.8×10^{-15}		
1423	2.7×10^{-15}		
1493	9.1×10^{-15}		

D_{Pt}

$D^\perp$, present MD study

T, K	D, m²/s	Q, eV	D_0, m²/s
1400	$(2.6 \pm 2.6) \times 10^{-20}$	4.67 ± 0.4	$((1.6 \pm 0.2) \times 10^{-3}$
1500	$(3.0 \pm 1.8) \times 10^{-19}$		
1600	$(3.3 \pm 1.2) \times 10^{-18}$		

$D\|$, present MD study

T, K	D, m²/s	Q, eV	D_0, m²/s
1400	$(0.5 \pm 2.6) \times 10^{-20}$	4.69 ± 0.4	$(3.79 \pm 1.6) \times 10^{-4}$
1500	$(0.6 \pm 1.8) \times 10^{-19}$		
1600	$(0.65 \pm 1.2) \times 10^{-18}$		

Experimental data

T, K	D, m²/s	Q, eV	D_0, m²/s
$\langle D \rangle$ determined for polycrystalline samples [9]			
1173	4.27×10^{-17}	3.03 ± 1.26	$2.1 (+3.9; -1.4) \times 10^{-4}$
1223	6.46×10^{-17}		
1273	2.45×10^{-16}		
1323	6.21×10^{-16}		
1373	9.6×10^{-16}		
1423	3.68×10^{-15}		
1473	9.27×10^{-15}		
1513	8.43×10^{-15}		
1543	3.28×10^{-14}		
1573	1.11×10^{-13}		
1603	5.06×10^{-14}		
1634	8.37×10^{-14}		
1663	1.58×10^{-13}		

time-dependent mean-square displacements $MSD_X^{\perp(\|)}(t)$ were determined by MD simulations. Exploration of the range of lower temperatures was not feasible because of the extremely long CPU time needed to record interpretable $MSD(t)$ curves.

Implementation of a simple model for vacancy thermodynamics allowed to account for the contribution of the temperature-dependent equilibrium vacancy concentration to the finally determined temperature dependence of $D_{Fe}^{\perp(\|)}$ and $D_{Pt}^{\perp(\|)}$. Generation of interpretable $MSD(t)$ curves required, however, that the simulated samples contain a sufficient number of vacancies. Hence, $D_{Fe}^{\perp(\|)}$ and $D_{Pt}^{\perp(\|)}$ (representing stationary self-diffusion) were determined by scaling the "raw" ones to the equilibrium vacancy concentration.

5.2. Evaluated diffusivities of Fe and Pt in view of the existing literature data

Table 3 presents an overview of the values of $D_{Fe}^{\perp(\|)}$ and $D_{Pt}^{\perp(\|)}$ determined by the present MD simulations and available experimental values reported in the literature.

As can be seen, the MD simulations revealed $D_{Fe}^{\perp(\|)} > D_{Pt}^{\perp(\|)}$ in the whole temperature range explored. The evaluated diffusivities are, however, considerably lower than the those reported in the cited experimental works. This could be attributed to the fact that while the simulated samples were ideal single crystals, real materials examined in the experiments might contain additional fast diffusion paths like grain boundaries, triple junctions, and dislocations. In addition, the impact of differences in the degree of $L1_0$ long-range order (most probably lower in the samples examined in real experiments) can neither be ignored.

The differences between the experimental and simulated values of $D_{Fe}^{\perp(\|)}$ and $D_{Pt}^{\perp(\|)}$ become somewhat reduced when considering the melting-point effect and the fact that diffusivities scale according to T/T_m [58,59]. As the value T_m of the melting point of FePt yielded by the MD simulations was higher than the experimental one, the comparison of the experimental and simulated values of diffusivities should be done by plotting them versus the reciprocal T/T_m with the simulated and experimental value of T_m, respectively. The related graphs are shown in Fig. 12c and d and it can be seen that although the simulated diffusivities
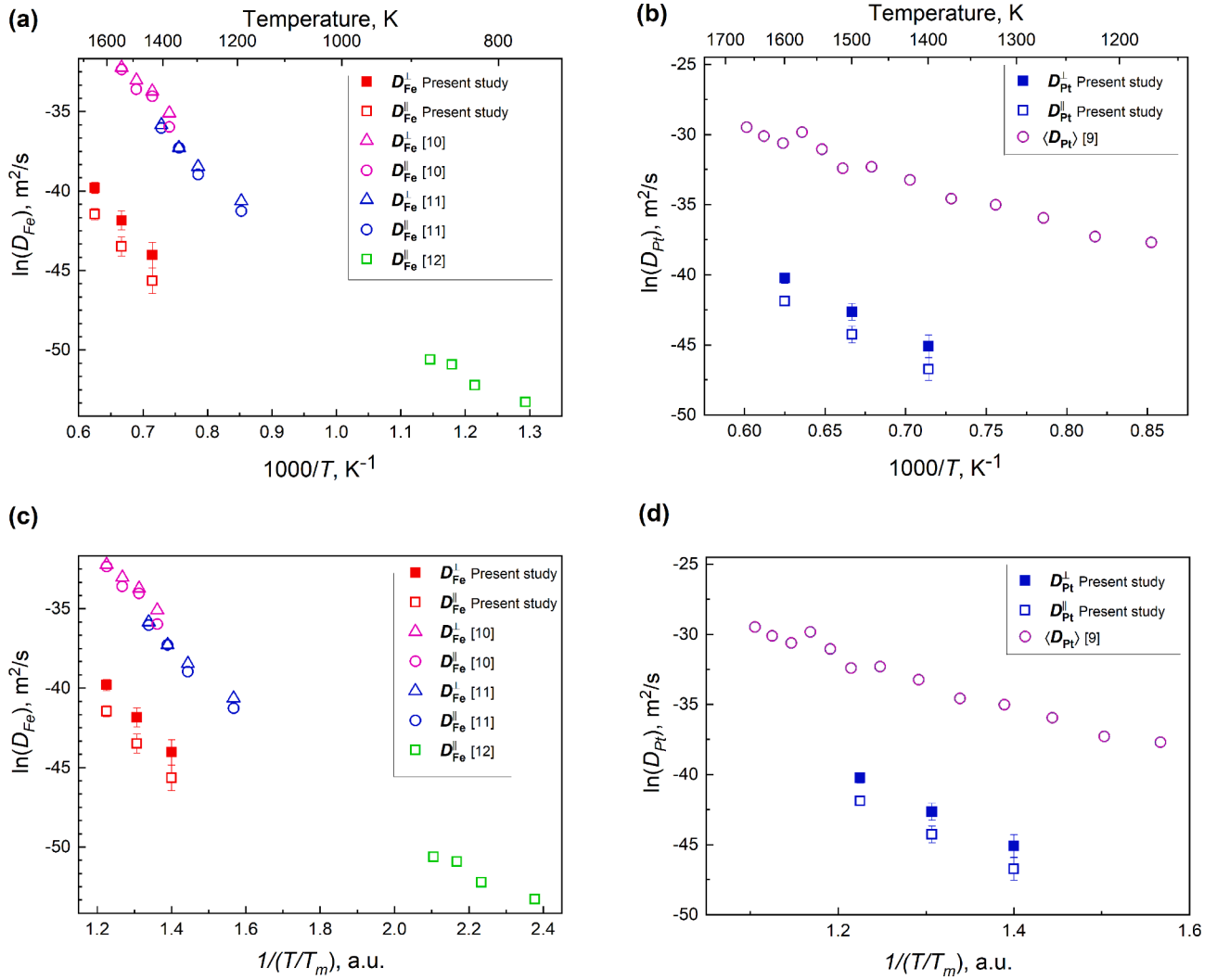
Fig. 12. Arrhenius plots of the experimental and simulated self-diffusion coefficients $D_{Fe(Pt)}^{\perp}$ (a, c) and $D_{Fe(Pt)}^{\parallel}$ (b, d) of $L1_0$-FePt. The graphs (c) and (d) show the Arrhenius plots traced vs. T/T_m with experimental and simulated values of T_m, respectively.
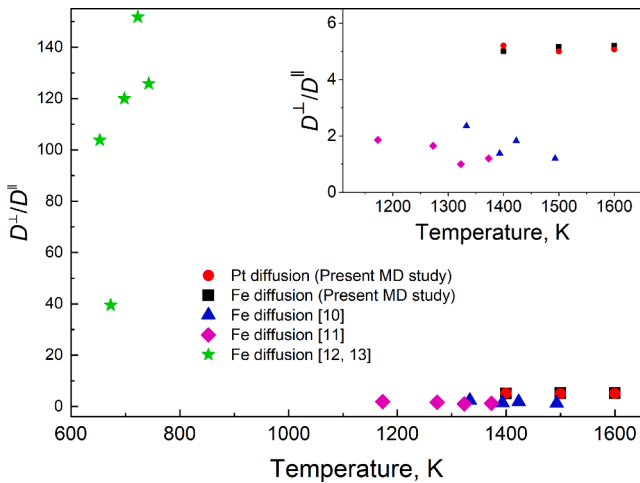

Fig. 13. Temperature dependence of the ratio $\frac{D_X^{\perp}}{D_X^{\parallel}}$. The MD results are compared to experimental values reported in the literature.

are still substantially lower than the experimental ones corresponding to the same T/T_m, the differences between the values are reduced with respect to those shown in Fig. 12a and b.

As mentioned in Section 2.5, further reduction of the differences between the simulated and experimental values of $D_{Fe(Pt)}$ is expected if the effect of the vacancy formation entropy S_V on the equilibrium vacancy concentrations $C_{V_x}^{eq}$ is taken into account.

The anisotropy of self-diffusion in $L1_0$-FePt, i.e. the relation $D_X^{\perp} > D_X\parallel$ (X = Fe; Pt) revealed by the present MD simulation, was previously observed in experimental studies [10,11,13]. Fig. 13 shows the degree of this anisotropy as a function of temperature and again our MD results are compared to experimental values reported in the literature [10–13].

The much higher value of $\frac{D_X\parallel}{D_X^{\perp}}$ measured at temperatures between 653 K and 743 K [13] should probably be attributed to a different dominant diffusion mechanism occurring at lower temperatures, as earlier suggested [12].

In contrary to the quantitative discrepancies between the experimental and MD results concerning the diffusivities, the activation energies, and the self-diffusion anisotropy, the simulations reproduced very well the experimental finding [10,11] which showed that the difference between the values of $D_{Fe}^{\perp}$ and $D_{Fe}\parallel$ was predominantly due to the difference between the pre-factors $D_0^{\perp}$ and $D_0\parallel$ (and not between the activation energies $Q_{Fe}^{\perp}$ and $Q_{Fe}\parallel$).

Table 4

Vacancy formation energies $E_V^{(X)}$ (X = Fe; Pt) in $L1_0$-FePt. Comparison of the present MD results with literature data.

	Present MD study	Kinetic Monte Carlo [65]	MD with analytic bond-order potential [60]	First principles [61]	First principles [62]
$E_V^{(Fe)}$	2.55 (300 K)	1.89	2.09	2.585	1.45
	2.53 (0 K)				
$E_V^{(Pt)}$	2.32 (300 K)	1.79	1.86	3.204	2.25
	2.31 (0 K)				

5.3. Reliability of the simulated vacancy formation energies

Table 4 shows the vacancy formation energies calculated in the present study (corresponding to $T = 300$ K and extrapolated to $T\rightarrow0$K) and related literature data. Substantial discrepancies between the reported literature data are conspicuous. While a MD study of FePt modelled with analytic bond-order potential [60] revealed $E_v^{(Fe)} > E_v^{(Pt)}$ in agreement with the present results, first principles studies suggest the opposite relationship [61,62]. In general, however, the values of the vacancy formation energies evaluated within the present work are higher than those reported in the literature. The gradual increase of vacancy formation energy with increasing temperature observed in the present MD simulations has been reported for a number of pure metals, e.g. bcc Fe [20], fcc Al [53], hcp and bcc Zr [54], and fcc Cu [63]. Moreover, a similar variation of the vacancy formation energy with temperature was found from *ab-initio* calculations performed for the disordered *A1*-FePt phase doped with Cu, Au, and Ag [64].

5.4. Thermodynamic activation energies

The self-diffusion coefficients $D_{Fe}^{\perp}$, $D_{Fe}\|$, $D_{Pt}^{\perp}$, and $D_{Pt}\|$ determined for three temperatures yielded reasonable Arrhenius plots (Figs. 11 and 12) allowing to estimate the corresponding activation energies $Q_X^{\perp\|}$ and the pre-factors $D_{0\_X}^{\perp\|}$ (X = Fe, Pt). In contrary to the self-diffusion coefficients D_X, the simulated values of $Q_{Fe}^{\perp\|}$ resulted generally in higher values than the corresponding experimental activation energies (see Table 3).

Since

$$D_X^{\perp(\|)}(T) = D_{0\_X}^{\perp(\|)} e^{-\frac{Q_X^{\perp(\|)}}{k_BT}} = D_{0\_X}^{\perp(\|)} e^{-\frac{E_V^{(Y)}+E_{m\_X}^{\perp(\|)}}{k_BT}} \qquad (13)$$

where $E_{m\_X}^{\perp(\|)}$ denotes the migration energy for X-atoms perpendicular ($\perp$) or along ($\|$) the [0 0 1] direction, the independently evaluated activation energies for self-diffusion ($Q_X^{\perp(\|)}$) and for vacancy formation ($E_V^{(X)}$) determine the values of $E_{m\_X}^{\perp(\|)}$. Such analysis whose results are displayed in Table 5 has been performed by applying the average activation energies $\langle E_V \rangle$ for Fe- and Pt-vacancy formation deduced from the Arrhenius plots of Fig. 7. The effect of the difference between the experimental and simulated value of the melting point of FePt (Section 4.2) has also been considered in this study.

As follows from Table 5, correction of temperature with respect to the melting point resulted in a general decrease of the simulated values of the activation energies $Q_{Fe(Pt)}^{\perp(\|)}$ for Fe and Pt self-diffusion in $L1_0$-FePt making them closer to the experimental ones (see Table 3).

It is remarkable that the relationship between the obtained values of the migration energies $E_m^{(Fe)}$ and $E_m^{(Pt)}$ is the same as the relationship between the migration energies of Fe and Pt in $L1_0$-FePt calculated directly by Kozlowski [66] who modelled the system using an analytic bond-order potential and determined the values $E_m^{(Fe)} = 2.26\ eV$ and $E_m^{(Pt)} = 3.12\ eV$ (averaged over different configurations of diffusion jumps) by analyzing saddle-point energies of the jumping atoms by means of Molecular Statics simulations.

6. Conclusions

Molecular Dynamics (MD) simulations were applied to investigate vacancy-mediated self-diffusion in a chemically $L1_0$-ordered FePt single crystal. Temperature dependent self-diffusion coefficients of Fe and Pt atoms were evaluated by a simulation algorithm implementing 'modified embedded-atom method' (MEAM) interaction potentials [31]. The simulated process of self-diffusion appeared anisotropic: both Fe and Pt atoms migrated approximately 5 times faster perpendicular to the [0 0 1] direction than parallel to it. The temperature dependences of the evaluated self-diffusion coefficients satisfied the Arrhenius law, however, the values of the self-diffusion coefficients were substantially lower and the related activation energies substantially higher than experimental values reported in the literature. It is supposed that the discrepancies are due to the existence of fast diffusion paths in real materials in contrast to the simulated ideal crystals. Discussing other possible sources of the discrepancies, two factors were considered: (i) the effect of the simulated value of the melting point of FePt being higher than the experimental one and (ii) the effect of the negligence of the vacancy formation entropy in the calculation of the equilibrium vacancy concentration. It was shown that correction of the results with respect to both factors leads to a reduction of the discrepancies between the simulated and experimental results. The MD simulation results allowed to evaluate a number of energetic parameters related to the vacancy-mediated atomic migration: the temperature dependent vacancy formation energies, the activation energies for self-diffusion, as well as the migration energies of the vacancy-mediated atomic migration.

Table 5

Simulated values of the activation energies for self-diffusion ($Q_X^{\perp\|}$), average activation energies for vacancy formation ($\langle E_V \rangle$) and the migration energies of X-atoms $E_{m\_X}^{\perp\|}$ in $L1_0$-FePt moving perpendicular ($\perp$) or along ($\|$) the [0 0 1] direction. The two sets of values were obtained with and without the correction with respect to the experimental and simulated value of the melting point T_m of FePt.

X	$Q_X^{\perp}$, eV	$\langle E_V \rangle$, eV	$E_{m\_X}^{\perp} = Q_X^{\perp} - E_v$, eV	$Q_X\|$, eV	E_v, eV	$E_{m\_X}\| = Q_X\| - E_v$, eV
Values yielded by the Arrhenius plots $ln(D_X)$ vs. T^{-1}						
Fe	4.09 ± 0.3	2.58 ± 0.05	1.51 ± 0.35	4.06 ± 0.3	2.58 ± 0.05	1.48 ± 0.35
Pt	4.67 ± 0.4	2.37 ± 0.05	2.30 ± 0.45	4.69 ± 0.4	2.37 ± 0.05	2.32 ± 0.45
Values yielded by the Arrhenius plots $ln(D_X)$ vs. $(T/T_m)^{-1}$						
Fe	3.84 ± 0.3	2.58 ± 0.05	1.26 ± 0.35	3.81 ± 0.3	2.58 ± 0.05	1.23 ± 0.35
Pt	4.38 ± 0.4	2.37 ± 0.05	2.01 ± 0.45	4.41 ± 0.4	2.37 ± 0.05	2.04 ± 0.45

for Fe and Pt atoms in $L1_0$-FePt single crystals.

The presented study showed that with the contemporary computational facilities vacancy-mediated atomic migration can be successfully simulated by means of MD algorithms. This conclusion seems very important, because when compared with standard Kinetic Monte Carlo techniques, the MD method enables much deeper insight into the physical phenomena accompanying diffusion processes on the atomic scale. One of the most important advantages of the MD method is a definite abandoning of the rigid lattice approximation which opens up opportunities for dynamical modelling of mutual influences between atomic migration and generation of lattice defects. Up to now, atomistic simulations of such effects were a domain of hybrid Kinetic Monte Carlo/Molecular Dynamics/Molecular Statics simulations, whose thermodynamic correctness was, however, not entirely proven. The possibility for covering large time scales by means of pure MD algorithms will provide a much more reliable tool for this task.

CRediT authorship contribution statement

S.I. Konorev: Data curation, Formal analysis, Investigation, Methodology, Software. **R. Kozubski:** Methodology, Conceptualization, Writing - review & editing. **M. Albrecht:** Funding acquisition, Project administration, Writing - review & editing. **I.A. Vladymyrskyi:** Conceptualization, Investigation, Funding acquisition, Project administration, Writing - original draft, Writing - review & editing.

Declaration of Competing Interest

The authors declare that they have no known competing financial interests or personal relationships that could have appeared to influence the work reported in this paper.

Acknowledgment

Appendix A. Supplementary data

Supplementary data to this article can be found online at https://doi.org/10.1016/j.commatsci.2021.110337.

References

[1] R. Würschum, S. Herth, U. Brossmann, Diffusion in nanocrystalline metals and alloys – A status report, Adv. Eng. Mater. 5 (5) (2003) 365–372.

[2] M. Albrecht, C. Brombacher, Rapid thermal annealing of FePt thin films, Phys. Status Solidi A 210 (7) (2013) 1272–1281.

[3] D. Weller, G. Parker, O. Mosendz, et al., Review article: FePt heat assisted magnetic recording media, J. Vac. Sci. Technol. B 34 (2016), 060801.

[4] O.V. Shamis, N.Y. Safonova, M.M. Voron, A.P. Burmak, S.I. Sidorenko, G.L. Katona, S. Gulyas, D.L. Beke, M. Albrecht, I.A. Vladymyrskyi, Phase transformations in Pt/Fe bilayers during post annealing probed by resistometry, J. Phys.: Condens. Matter 31 (28) (2019) 285401, https://doi.org/10.1088/1361-648X/ab169c.

[5] K. Hono, Y.K. Takahashi, G. Ju, J.-U. Thiele, A. Ajan, X.M. Yang, R. Ruiz, L. Wan, Heat-assisted magnetic recording media materials, MRS Bull. 43 (2) (2018) 93–99.

[6] M.T. Kief, R.H. Victora, Materials for heat-assisted magnetic recording, MRS Bull. 43 (2) (2018) 87–92.

[7] J. Wang, H. Sepehri-Amin, H. Tajiri, et al., Impact of carbon on microstructure and magnetic properties of FePt-C nanogranular films on MgO substrate, Acta Mater. 166 (2019) 413–423.

[8] I. Suzuki, J. Wang, Y.K. Takahashi, et al., Control of grain density in FePt-C granular thin films during initial growth, J. Magn. Magn. Mater. 500 (2020), 166418.

[9] J. Kučera, B. Million, Diffusion of Platinum in the Fe-Pt System, Phys. Stat. Sol. A 31 (1) (1975) 275–282.

[10] A. Kushida, K. Tanaka, H. Numakura, Chemical diffusion in $L1_0$-ordered FePt, Mater. Trans. 44 (2003) 59–62.

[11] Y. Nosé, T. Ikeda, H. Nakajima, et al., Tracer diffusion of Fe and Pd in FePt and $FePt_3$, Defect Diffus. Forum 237 (2005) 450–455.

[12] M. Rennhofer, B. Sepiol, M. Sladecek, et al., Self-diffusion of iron in $L1_0$-ordered FePt thin films, Phys. Rev. B 74 (2006), 104301.

[13] F. Gröstlinger, M. Rennhofer, M. Leitner, et al., Anisotropic diffusion in FePt thin films, Phys. Rev. B 85 (2012), 134302.

[14] I.O. Kruhlov, O.V. Shamis, N.Y. Schmidt, M.V. Karpets, S. Gulyas, E. Hadjixenophontos, A.P. Burmak, S.I. Sidorenko, G.L. Katona, G. Schmitz, M. Albrecht, I.A. Vladymyrskyi, Structural phase transformations in annealed Pt/Mn/Fe trilayers, J. Phys.: Condens. Matter 32 (36) (2020) 365404, https://doi.org/10.1088/1361-648X/ab9269.

[15] I.O. Kruhlov, O.V. Shamis, N.Y. Schmidt, et al., Thermally-induced phase transitions in Pt/Tb/Fe trilayers, Thin Solid Films 709 (2020), 138134.

[16] G.L. Katona, I.A. Vladymyrskyi, I.M. Makogon, S.I. Sidorenko, F. Kristály, L. Daróczi, A. Csik, A. Liebig, G. Beddies, M. Albrecht, D.L. Beke, Grain boundary diffusion induced reaction layer formation in Fe/Pt thin films, Appl. Phys. A 115 (1) (2014) 203–211.

[17] D.L. Beke, Yu. Kaganovskii, G.L. Katona, Interdiffusion along grain boundaries – Diffusion induced grain boundary migration, low temperature homogenization and reactions in nanostructured thin films, Prog. Mater. Sci. 98 (2018) 625–674.

[18] I.A. Vladymyrskyi, A.E. Gafarov, A.P. Burmak, et al., Low-temperature formation of the FePt phase in the presence of an intermediate Au layer in Pt/Au/Fe thin films, J. Phys. D: Appl. Phys. 49 (2016), 035003.

[19] Y. Mishin, Atomistic computer simulation of diffusion, chapter 3, in: D. Gupta (Ed.), Diffusion Processes in Advanced Technological Materials, Springer, NY, 2005:113..

[20] M.I. Mendelev, Y. Mishin, Molecular dynamics study of self-diffusion in bcc Fe, Phys. Rev. B 80 (2009), 144111.

[21] D.E. Smirnova, A.Y. Kuksin, S.V. Starikov, Investigation of point defects diffusion in bcc uranium and U-Mo alloys, J. Nucl. 458 (2015) 304–311.

[22] A. Einstein, Annalen der Physik 17 (1905) 549.

[23] M. von Smoluchowski, Annalen der Physik 21 (1906) 756.

[24] S. Plimpton, Fast parallel algorithms for short-range molecular dynamics, J. Comput. Phys. 117 (1) (1995) 1–19.

[25] LAMMPS, https://lammps.sandia.gov/.

[26] H. Bakker, Tracer diffusion in concentrated alloys, in: G.E. Murch, A.S. Nowick (Eds.), Diffusion in Crystalline Solids, Academic Press, Orlando, 1984, pp. 189–256.

[27] J. Betlej, P. Sowa, R. Kozubski, et al., Self-diffusion in a triple-defect A-B binary system: Monte Carlo simulation, Comput. Mater. 172 (2020), 109316.

[28] T.R. Mattsson, A.E. Mattsson, Calculating the vacancy formation energy in metals: Pt, Pd, and Mo, Phys. Rev. B 66 (21) (2002), https://doi.org/10.1103/PhysRevB.66.214110.

[29] Y. Gong, B. Grabowski, A. Glensk, et al., Temperature dependence of the Gibbs energy of vacancy formation of fcc Ni, Phys. Rev. B 97 (2018), 214106.

[30] J.J. Burton, Vacancy-formation entropy in cubic metals, Phys. Rev. B 5 (1972) 2948.

[31] J. Kim, Y. Koo, B.-J. Lee, Modified embedded-atom method interatomic potential for the Fe–Pt alloy system, J. Mater. Res. 21 (1) (2006) 199–208.

[32] Z.S. Basinski, W. Hume-Rothery, A.L. Sutton, The lattice expansion of iron, Proc. R. Soc. Lond. A 229 (1955) 459–467.

[33] J.R. Morris, C.Z. Wang, K.M. Ho, et al., Melting line of aluminum from simulations of coexisting phases, Phys. Rev. B. 49 (1994) 3109.

[34] Y. Nosé, A. Kushida, T. Ikeda, H. Nakajima, K. Tanaka, H. Numakura, Re-examination of phase diagram of Fe-Pt system, Mater. Trans. 44 (12) (2003) 2723–2731.

[35] I. Seki, K. Nagata, Lattice constant of iron and austenite including its supersaturation phase of carbon, ISIJ Int. 45 (2005) 1789–1794.

[36] Handbook of Chemistry and Physics, 94th ed., CRC Press, 2013.

[37] W. Zhong, G. Overney, D. Toma'nek,, Structural properties of Fe crystals, Phys. Rev. B 47 (1993) 95.

[38] C. Kittel, Introduction to Solid State Physics, 5th ed., Wiley, New York, 1976.

[39] G K White, Thermal expansion of magnetic metals at low temperatures, Proc. Phys. Soc. 86 (1) (1965) 159–169.

[40] J.W. Edwards, R. Speiser, and H.L. Johnston, High temperature structure and thermal expansion of some metals as determined by X-ray diffraction data. I. Platinum, tantalum, niobium, and molybdenum, J. Appl. Phys. 22 (1951) 424-428.

[41] Y. Waseda, K. Hirata, M. Ohtani, High-temperature thermal expansion of platinum, tantalum, molybdenum, and tungsten measured by X-ray diffraction, High Temp. - High Pressures 7 (1975) 221–226.

[42] E.H. Abdul-Hafidh, B. Aissa, Predictions of the mechanical and structural properties of spherical platinum nanoparticles by Chen-Mobius lattice inversion method, J. Comput. Theor. Nanos. 12 (12) (2015) 5076–5080.

[43] J.W. Arblaster, Crystallographic properties of platinum, Platin. Met. Rev. 41 (1997) 12–21.

[44] J.B. Austin, A vacuum apparatus for measuring thermal expansion at elevated temperatures, with measurements on platinum, gold, magnesium and zinc, Physics 3 (5) (1932) 240–267.

[45] Z. Bamshad, S.A. Sebt, M.R. Abolhassani, Size control of $L1_2$-FePt$_3$ nanocrystals by spin-coating method, J. Theor. Appl. Phys. 10 (3) (2016) 251–257.

[46] L. Suber, P. Imperatori, E.M. Bauer, R. Porwal, D. Peddis, C. Cannas, A. Ardu, A. Mezzi, S. Kaciulis, A. Notargiacomo, L. Pilloni, Tuning hard and soft magnetic FePt nanocomposites, J. Alloy Compd. 663 (2016) 601–609.

[47] K. Tajima, Y. Endoh, Y. Ishikawa, et al., Acoustic-phonon softening in the Invar alloy Fe$_3$Pt, Phys. Rev. Lett. 37 (1976) 519.

[48] Y.-F. Jia, X.-L. Shu, Y. Xie, Z.-Y. Chen, Physical properties of FePt nanocomposite doped with Ag atoms: First-principles study, Chinese Phys. B 23 (7) (2014) 076105, https://doi.org/10.1088/1674-1056/23/7/076105.

[49] K. Sato, Y. Hirotsu, Magnetoanisotropy, long-range order parameter and thermal stability of isolated L1$_0$ FePt nanoparticles with mutual fixed orientation, J. Magn. Magn. Mater. 272-276 (2004) 1497–1499.

[50] S. Kim, Issues on the choice of a proper time step in molecular dynamics, Phys. Procedia 53 (2014) 60–62.

[51] R. Nicula, O. Crisan, A.D. Crisan, I. Mercioniu, M. Stir, F. Vasiliu, Thermal stability, thermal expansion and grain-growth in exchange-coupled Fe–Pt–Ag–B bulk nanocomposite magnets, J. Alloy Compd. 622 (2015) 865–870.

[52] O. Crisan, A.D. Crisan, I. Mercioniu, D. Pantelica, A. Pantelica, S. Vaucher, R. Nicula, M. Stir, F. Vasiliu, Effect of Mn addition on the thermal stability and magnetic properties of rapidly-quenched L1$_0$ FePt alloys, Intermetallics 65 (2015) 81–87.

[53] B.S. Bokstein, A. Epishin, V. Esin, M. Mendelev, A. Rodin, S. Zhevnenko, Cross diffusion-stresses effects, Defect Diffus. Forum 264 (2007) 79–89.

[54] M.I. Mendelev, B.S. Bokstein, Molecular dynamics study of self-diffusion in Zr, Philos. Mag. 90 (5) (2010) 637–654.

[55] M.G. Del Pópolo, G.A. Voth, On the Structure and Dynamics of Ionic Liquids, J. Phys. Chem. B 108 (5) (2004) 1744–1752.

[56] T.B. Schrøder, J.C. Dyre, Solid-like mean-square displacement in glass-forming liquids, J. Chem. Phys. 152 (2020), 141101.

[57] P. Sowa, R. Kozubski, A. Biborski, et al., Self-diffusion and "order-order" kinetics in B2-ordering AB binary systems with a tendency for triple defect formation: Monte Carlo simulation, Philos. Mag. 93 (2013) 1987–1998.

[58] G.P. Tivari, R.S. Mehrotra, Diffusion and melting, Def. Diff. Forum 279 (2008) 23–37.

[59] N. Matsuura, G.M. Hood, H. Zou, The correspondence between self-diffusion properties and melting temperatures for α-Zr and α-TiJ, Nucl. Mater. 238 (1996) 260–263.

[60] H. Dong, X.L. Shu, R.M. Wang, Point defects in L1$_0$ FePt studied by molecular dynamics simulations based on an analytic bond-order potential, Sci. China Phys. Mech. Astron. 54 (8) (2011) 1429–1432.

[61] Y. Sui, Z.Y. Chen, X.L. Shu, et al., Point defects in L1$_0$ phase FePt alloy: a first principle study, Mater. Sci. Forum 561–565 (2007) 1923–1926.

[62] X.L. Shu, Z.Y. Chen, Q. Chen, W.Y. Hu, The effect of vacancy created by ion irradiation on the ordering of FePt: A first-principle study, Nucl. Instrum. Meth. B 267 (18) (2009) 3271–3273.

[63] M.I. Mendelev, M.J. Kramer, C.A. Becker, M. Asta, Analysis of semi-empirical interatomic potentials appropriate for simulation of crystalline and liquid Al and Cu, Philos. Mag. 88 (12) (2008) 1723–1750.

[64] H.B. Luo, J. Du, A.R. Yan, J.P. Liu, A theoretical study of thermal vacancy formation enthalpy of disordered FePt doped by Cu, Zn and Ag, Comput. Mater. 144 (2018) 120–125.

[65] M. Müller, K. Albe, Kinetic lattice Monte-Carlo simulations on the ordering kinetics of free and supported FePt L1$_0$-nanoparticles, Beilstein J. Nanotechnol. 2 (2011) 40–46.

[66] M. Kozlowski, Kinetics of structural transformations in bulk and nano-layered intermetallic systems with L10 superstructure, Thesis submitted for the degree of Doctor of Philosophy (2010). https://fais.uj.edu.pl/documents/41628/0207353f-81cc-4a94-b094-bf7037d72174.